Supporting Information for

Photo-controllable Heterostructured Crystal of Metal-Organic Framework via Reversible Photocycloaddition

Xin-Da Huang,[a‡] Ben-Kun Hong,[b‡] Ge-Hua Wen,[a] Shu-Hua Li*[b] and Li-Min Zheng*[a]

[a]State Key Laboratory of Coordination Chemistry, School of Chemistry and Chemical Engineering, Collaborative Innovation Centre of Advanced Microstructures, Nanjing University, Nanjing 210023, P. R. China.

[b]Institute of Theoretical and Computational Chemistry, School of Chemistry and Chemical Engineering, Nanjing University, Nanjing 210023, China.

[‡]These authors contributed equally to this work.

*E-mail: lmzheng@nju.edu.cn, shuhua@nju.edu.cn

Contents

I. Experimental section

General materials and measurements. The ligand of $depma_2$ was synthesized according to the literature.[1] All other starting materials were of analytical grade obtained from commercial sources and used without any purification. PE 240C analyser were carried out to do the elemental analyses for C, H and N. The instrument to collect powder X-ray diffraction (PXRD) data was Bruker D8 advance diffractometer with Cu-K_α radiation in a range of 5-50°. The Fourier infrared spectra were attained from Bruker Tensor 27 spectrometer in 4000-600 cm^{-1} region. Thermogravimetric (TG) analyses were collected on a Mettler Toledo TGA/DSC 1 instrument in the range of 30-600 °C under a nitrogen flow (20 mL/min) at a heating rate of 5 °C min^{-1}. The determination of differential scanning calorimetry (DSC) was conducted on Mettler DSC823e instrument. The UV/Vis spectra were measured on a Perkin Elmer Lambda 950 UV/VIS/NIR spectrometer using powder samples. All measurements related to the photochemical reactions were performed upon irradiation with 280 or 365 nm LED UV light (50 W *IUVOT* UV lamp, powder setting: 20% power, power density: ca. 100 mW cm^{-2}).

X-ray crystallography. Single crystals were used for data collections on a Bruker D8 Venture diffractometer using graphite-monochromated Mo-K*α* radiation (λ = 0.71073 Å) for compounds **1**, **2** and **3**, or a Bruker D8 Liquid Metal-jet diffractometer using Ga Kα radiation (λ=1.34139 Å) for reverse **2**. The data were integrated using the Siemens SAINT program,[2] with the intensities corrected for Lorentz factor, polarization, air absorption, and absorption due to variation in the path length through the detector faceplate. Empirical absorption corrections were applied using the SADABS program.[3] The structures were solved by direct method and refined on F^2 by full-matrix least squares using SHELXTL.[4] All the non-hydrogen atoms were refined anisotropically. All hydrogen atoms were located in a difference map, added geometrically, and isotropically refined with a riding model. The residual electron densities were of no chemical significance. CCDC 2214247-2214250 contain the supplementary crystallographic data for this paper. These data can be obtained free of charge from the Cambridge Crystallographic Data Centre via www.ccdc.cam.ac.uk/data_request/cif.

General photoluminescent measurement. The steady fluorescence spectra were attained at Bruker Spectrofluorimeter LS55. Time-resolved emission decays and absolute photoluminescent quantum yield (PLQY) were carried out on Fluorolog-3 spectrofluorometer (Horiba Scientific). Nanosecond lifetime decays were conducted using a TCSPC MCA model equipped with a picosecond photodetector (<200 ps) (PPD850) and picosecond laser (duration is 180 ps, Deltadiode, 100 MHz laser). Microsecond lifetime decays were collected by a MCS mode on TCSPC HUB (DeltaHUB) with a LED source (SpectraLED) as a sample excitation source. All decay profiles are fitted reasonably to a single or double exponential function using the software DAS6 attached to FluoroLog-UltraFast (HORIBA Instrument Inc, Edison) to give lifetime.

Optical microscopy measurements. As for the experiments of fabricating heterostructure crystals and photo-inducing crystal deformation of rod-like crystals, the optical images and movies were collected using Caikang XPF-550C polarization microscope equipped with LED UV lamp (*IUVOT* 50 W).

Synthesis of $[Dy(NO_3)_3(depma_2)_{1.5}]\cdot(depma_2)_{0.5}\cdot CH_3OH$ (1). A 5 mL methanol solution dissolved with $Dy(NO_3)_3\cdot 6H_2O$ (0.05 mmol, 22.8 mg) was mixed with 5 mL CH_2Cl_2 containing $depma_2$ (0.1 mmol, 65.6 mg) and was then left at room temperature for three days to afford colorless rod-like crystals with a yield of 50.2 mg (56.7 %). Notably, uniform needle-like crystals for photochemical researches were isolated from the 10 mL methanol solution after the slow evaporation for two weeks. Elemental anal. Calcd (%): C, 54.60; H, 5.24; N, 2.48. Found (%): C, 54.43; H, 5.21; N, 2.22. IR (cm^{-1}): 3395(w), 3070(vw), 3040(vw), 2987(w), 2927(w), 2905(vw), 2865(vw), 1734(vw), 1632(w), 1517(w), 1493(m), 1474(s), 1453(m), 1424(w), 1393(w), 1368(w), 1293(s), 1258(w), 1206(m), 1180(s), 1150(m), 1100(w), 1096(w), 1050(vs), 1025(vs), 987(w), 972(w), 948(w), 873 (w), 814(vw), 802(vw), 781(m), 765(w), 744(w), 718(w), 688(m), 645(w).

Synthesis of $[Dy(NO_3)_3(depma_2)_{1.5}]\cdot(depma_2)_{0.5}$ (2). The desolvation phase **2** can be obtained by keep compound **1** in air for several days or thermal annealing at 80°C for 10 min. Elemental anal. Calcd (%): C, 54.40; H, 5.05; N, 2.50. Found (%): C, 53.98; H, 5.16; N, 2.55.

Synthesis of $[Dy(NO_3)_3(depma)(depma_2)]\cdot(depma_2)_{0.5}$ (3). The thermal annealing of compound **1** or **2** at 140°C for 5 min provided compound **3**. Elemental anal. Calcd (%): C, 54.40; H, 5.05; N, 2.50. Found (%): C, 54.25; H, 5.10; N, 2.46.

II. Single-crystal-to-single-crystal structural transformation

Table S1. Crystallographic data for **1**, **2**, **3** and reversed **2** from exposure of **3** to 365 nm UV light.

Compounds	**1**	**2**	**3**	reversed **2**
Empirical formula	$C_{77}H_{88}DyN_3O_{22}P_4$		$C_{76}H_{84}DyN_3O_{22}P_4$	
Temperature (K)	193(2)	193(2)	193(2)	193(2)
fw (g mol^{-1})	1693.88	1661.84	1661.84	1661.84
Crystal system	Triclinic	Triclinic	Triclinic	Triclinic
Space group	$P\bar{1}$	$P\bar{1}$	$P\bar{1}$	$P\bar{1}$
a (Å)	12.0582(4)	12.0168(18)	12.1321(10)	12.0667(5)
b (Å)	13.8579(5)	13.485(2)	13.3341(10)	13.4722(6)
c (Å)	23.2328(8)	23.445(3)	23.3083(17)	23.4814(10)
α (°)	90.6460(10)	90.470(6)	90.473(3)	90.745(2)
β (°)	97.9700(10)	97.255(4)	95.995(3)	97.128(2)
γ (°)	86.0330(10)	93.184(6)	92.718(3)	93.145(2)
V (Å^3)	3835.5(2)	3762.6(10)	3745.4(5)	3781.3(3)
Z	2	2	2	2
ρ_{calcd} (g cm^{-3})	1.467	1.467	1.474	1.460
F(000)	1746	1710	1710	1710
goodness-of-fit on F^2	1.040	1.080	1.095	1.140
R_1, wR_2 [I >2σ(I)][a]	0.0504, 0.1148	0.0690, 0.1765	0.0581, 0.1485	0.0755, 0.2062
R_1, wR_2 (all data)[a]	0.0697, 0.1222	0.0921, 0.1954	0.0827, 0.1704	0.0941, 0.2204
CCDC number	2214247	2214250	2214249	2214248

[a] $R_1 = \Sigma||F_o| - |F_c||/\Sigma|F_o|$, $wR_2 = [\Sigma w(F_o^2 - F_c^2)^2/\Sigma w(F_o^2)^2]^{1/2}$

Table S2. Selected bond lengths (Å) and angles (°) for compound **1** at 193 K.

Dy1-O1	2.302(3)	O4-Dy1-O14	146.66(17)
Dy1-O4	2.295(4)	O4-Dy1-O16	74.61(12)
Dy1-O7	2.329(3)	O4-Dy1-O17	126.22(12)
Dy1-O10	2.433(4)	O7-Dy1-O10	73.42(12)
Dy1-O11	2.465(5)	O7-Dy1-O11	124.54(13)
Dy1-O13	2.414(4)	O7-Dy1-O13	75.09(10)
Dy1-O14	2.465(4)	O7-Dy1-O14	124.04(14)
Dy1-O16	2.487(3)	O7-Dy1-O16	77.29(12)
Dy1-O17	2.441(4)	O7-Dy1-O17	80.42(13)
C2-C9A	1.638(6)	O10-Dy1-O11	51.14(14)
C21-C28B	1.634(5)	O10-Dy1-O13	73.41(13)
C40-C47C	1.640(6)	O10-Dy1-O14	100.06(15)
C59-C66D	1.638(7)	O10-Dy1-O16	140.09(13)
O1-Dy1-O4	82.16(12)	O10-Dy1-O17	143.89(12)
O1-Dy1-O7	153.18(11)	O11-Dy1-O13	88.99(15)
O1-Dy1-O10	127.60(13)	O11-Dy1-O14	73.26(17)
O1-Dy1-O11	78.13(13)	O11-Dy1-O16	145.98(13)
O1-Dy1-O13	123.61(10)	O11-Dy1-O17	146.89(14)
O1-Dy1-O14	73.00(13)	O13-Dy1-O14	50.82(13)
O1-Dy1-O16	76.11(12)	O13-Dy1-O16	123.89(14)
O1-Dy1-O17	85.72(13)	O13-Dy1-O17	76.13(13)
O4-Dy1-O7	87.66(13)	O14-Dy1-O16	118.81(15)
O4-Dy1-O10	77.67(12)	O14-Dy1-O17	74.44(17)
O4-Dy1-O11	80.23(14)	O16-Dy1-O17	51.62(12)
O4-Dy1-O13	149.49(12)		

Symmetry codes: A: -x, 2-y, 2-z; B: 1-x, 1-y, 2-z**;** C: 1-x, 2-y, 1-z; D: -x, 1-y, 1-z.

Table S3. Selected bond lengths (Å) and angles (°) for compound **2** at 193 K.

Dy1-O1	2.289(5)	O4-Dy1-O14	148.7(2)
Dy1-O4	2.288(5)	O4-Dy1-O16	73.95(17)
Dy1-O7	2.327(5)	O4-Dy1-O17	125.52(16)
Dy1-O10	2.424(5)	O7-Dy1-O10	73.86(17)
Dy1-O11	2.452(6)	O7-Dy1-O11	125.47(18)
Dy1-O13	2.424(5)	O7-Dy1-O13	76.60(17)
Dy1-O14	2.479(5)	O7-Dy1-O14	123.18(19)
Dy1-O16	2.481(5)	O7-Dy1-O16	77.21(18)
Dy1-O17	2.454(5)	O7-Dy1-O17	78.24(17)
C2-C9A	1.634(7)	O10-Dy1-O11	51.69(19)
C21-C28B	1.627(8)	O10-Dy1-O13	73.66(17)
C40-C47C	1.622(9)	O10-Dy1-O14	105.59(18)
C59-C66D	1.657(14)	O10-Dy1-O16	140.0(2)
O1-Dy1-O4	81.40(18)	O10-Dy1-O17	142.75(16)
O1-Dy1-O7	153.46(16)	O11-Dy1-O13	85.0(2)
O1-Dy1-O10	126.53(17)	O11-Dy1-O14	75.4(2)
O1-Dy1-O11	77.59(19)	O11-Dy1-O16	148.0(2)
O1-Dy1-O13	122.57(18)	O11-Dy1-O17	145.41(18)
O1-Dy1-O14	71.63(17)	O13-Dy1-O14	51.01(1 7)
O1-Dy1-O16	76.52(18)	O13-Dy1-O16	125.20(18)
O1-Dy1-O17	88.35(17)	O13-Dy1-O17	76.26(17)
O4-Dy1-O7	87.88(18)	O14-Dy1-O16	113.3(2)
O4-Dy1-O10	77.86(16)	O14-Dy1-O17	70.2(2)
O4-Dy1-O11	83.82(19)	O16-Dy1-O17	51.67(17)
O4-Dy1-O13	150.37(17)		

Symmetry codes: A: -x, -y, -z; B: 1-x, 2-y, 1-z; C: -x, 2-y, 2-z; D: 1-x, 1-y, 2-z.

Table S4. Selected bond lengths (Å) and angles (°) for compound **3** at 193 K.

Dy1-O1	2.290(4)	O4-Dy1-O14	148.79(17)
Dy1-O4	2.298(4)	O4-Dy1-O16	73.17(14)
Dy1-O7	2.305(4)	O4-Dy1-O17	124.76(13)
Dy1-O10	2.418(5)	O7-Dy1-O10	73.52(14)
Dy1-O11	2.454(5)	O7-Dy1-O11	124.96(13)
Dy1-O13	2.427(5)	O7-Dy1-O13	75.71(16)
Dy1-O14	2.463(5)	O7-Dy1-O14	124.76(16)
Dy1-O16	2.487(4)	O7-Dy1-O16	77.45(14)
Dy1-O17	2.451(4)	O7-Dy1-O17	80.64(13)
C2-C9A	1.632(6)	O10-Dy1-O11	51.47(14)
C21-C28B	1.631(6)	O10-Dy1-O13	76.11(17)
C40-C47C	3.60(1)	O10-Dy1-O14	102.75(15)
C59-C66D	1.632(6)	O10-Dy1-O16	140.87(15)
O1-Dy1-O4	81.87(14)	O10-Dy1-O17	143.52(15)
O1-Dy1-O7	153.10(13)	O11-Dy1-O13	91.15(17)
O1-Dy1-O10	126.80(16)	O11-Dy1-O14	75.18(17)
O1-Dy1-O11	77.16(15)	O11-Dy1-O16	145.98(15)
O1-Dy1-O13	122.97(16)	O11-Dy1-O17	146.14(14)
O1-Dy1-O14	72.12(15)	O13-Dy1-O14	51.04(17)
O1-Dy1-O16	76.09(15)	O13-Dy1-O16	121.12(17)
O1-Dy1-O17	86.75(15)	O13-Dy1-O17	72.82(16)
O4-Dy1-O7	85.96(13)	O14-Dy1-O16	115.31(17)
O4-Dy1-O10	79.09(14)	O14-Dy1-O17	71.55(16)
O4-Dy1-O11	82.60(14)	O16-Dy1-O17	51.64(15)
O4-Dy1-O13	152.45(15)		

Symmetry codes: A: 1-x,1-y, -z; B: 1-x, 1-y, -z; C: -x, 1-y, 1-z; D: 1-x, -y, 1-z.

Table S5. Selected bond lengths (Å) and angles (°) for crystal of reversed **2** obtained from the exposure of **3** to 365 nm UV light for half an hour.

Dy1-O1	2.287(5)	O4-Dy1-O14	148.7(2)
Dy1-O4	2.305(6)	O4-Dy1-O16	74.0(2)
Dy1-O7	2.326(5)	O4-Dy1-O17	125.4(2)
Dy1-O10	2.431(5)	O7-Dy1-O10	73.7(2)
Dy1-O11	2.448(7)	O7-Dy1-O11	125.2(2)
Dy1-O13	2.415(7)	O7-Dy1-O13	77.2(2)
Dy1-O14	2.489(7)	O7-Dy1-O14	123.4(2)
Dy1-O16	2.482(7)	O7-Dy1-O16	77.5(2)
Dy1-O17	2.457(6)	O7-Dy1-O17	78.2(2)
C2-C9A	1.644(10)	O10-Dy1-O11	51.7(2)
C21-C28B	1.632(10)	O10-Dy1-O13	74.3(2)
C40-C47C	1.645(11)	O10-Dy1-O14	106.7(2)
C59-C66D	1.66(2)	O10-Dy1-O16	139.7(2)
O1-Dy1-O4	81.33(19)	O10-Dy1-O17	143.0(2)
O1-Dy1-O7	153.50(18)	O11-Dy1-O13	83.9(3)
O1-Dy1-O10	126.4(2)	O11-Dy1-O14	75.3(3)
O1-Dy1-O11	77.9(2)	O11-Dy1-O16	148.4(2)
O1-Dy1-O13	122.2(2)	O11-Dy1-O17	145.2(2)
O1-Dy1-O14	71.3(2)	O13-Dy1-O14	50.9(2)
O1-Dy1-O16	76.3(2)	O13-Dy1-O16	125.5(2)
O1-Dy1-O17	88.5(2)	O13-Dy1-O17	76.4(3)
O4-Dy1-O7	87.78(19)	O14-Dy1-O16	112.6(2)
O4-Dy1-O10	77.28(18)	O14-Dy1-O17	70.0(3)
O4-Dy1-O11	84.4(2)	O16-Dy1-O17	51.6(2)
O4-Dy1-O13	150.6(2)		

Symmetry codes: A: -x, -y, -z; B: 1-x, 2-y, 1-z; C: -x, 2-y, 2-z; D: 1-x, 1-y, 2-z.

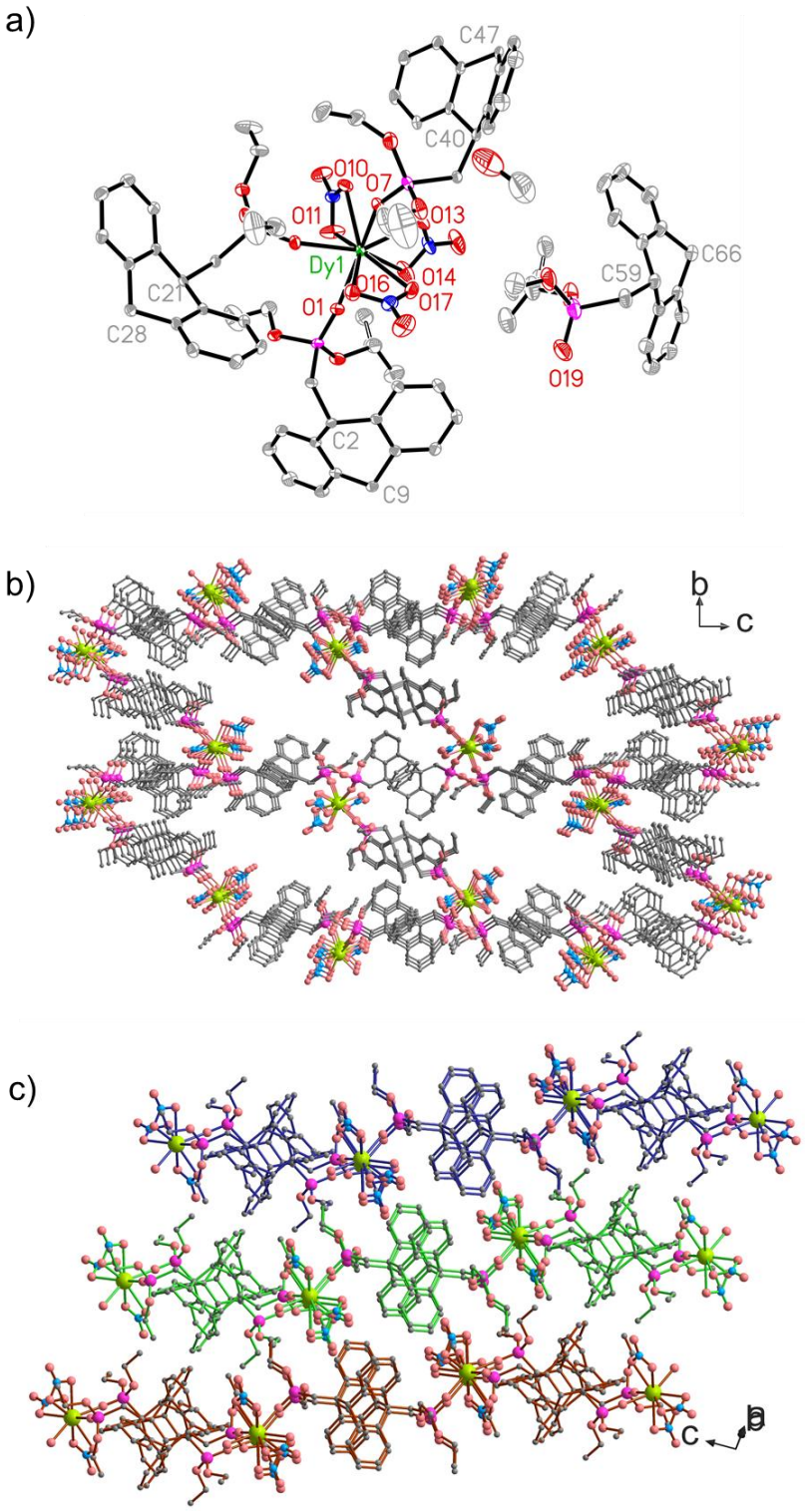

Fig. S1 The structure of **1**. (a) The asymmetric unit with 30% thermal ellipsoids. (b, c) The layer stacking in structure **1** viewed in different directions, the guest depma$_2$-D and methanol molecules are omitted to show clearly the channel along the *a*-axis.

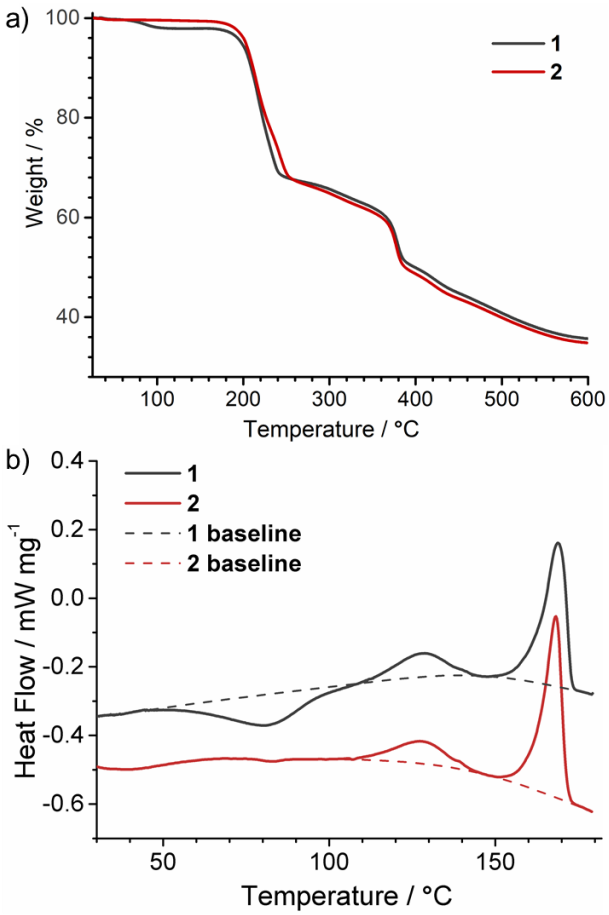

Fig. S2 (a) Thermogravimetric analyses and (b) DSC curves of **1** and **2** measured under nitrogen atmosphere at a heating rate of 5 °C/min.

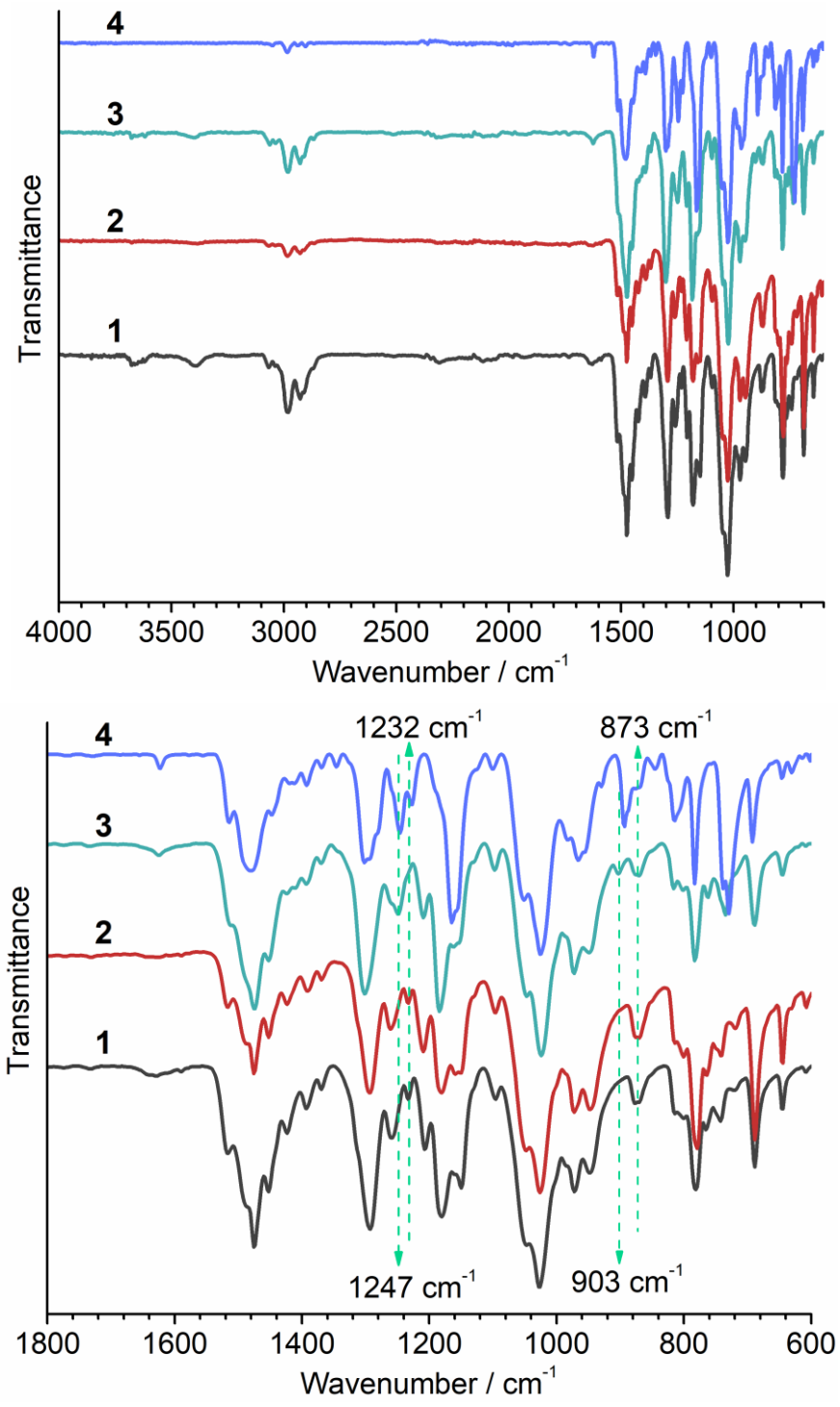

Fig. S3 The FTIR spectra for the samples of **1** (black), **2** (red), **3** (green) and **4** (blue).

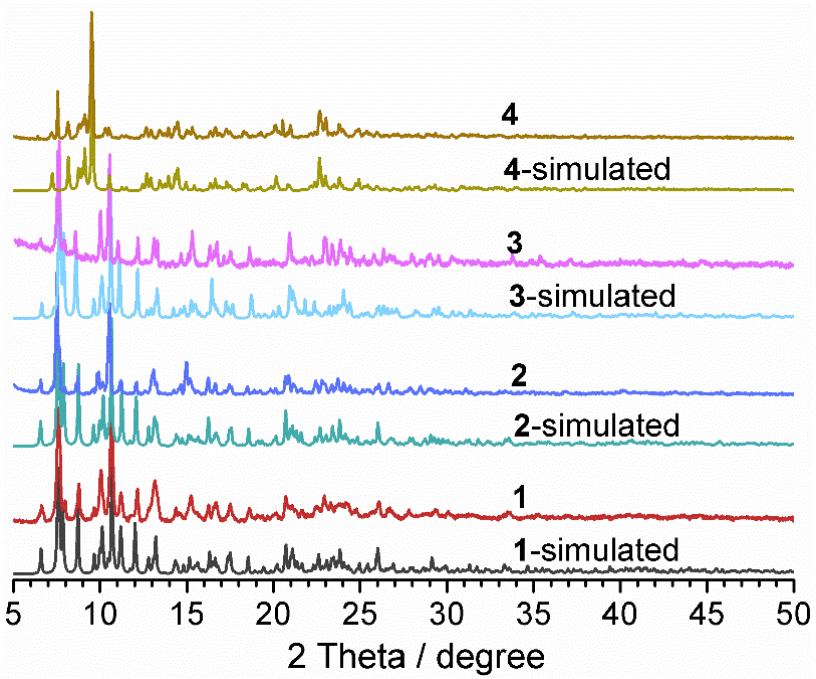

Fig. S4 The experimental and simulated PXRD patterns for compounds **1**, **2**, **3**, and **4**.

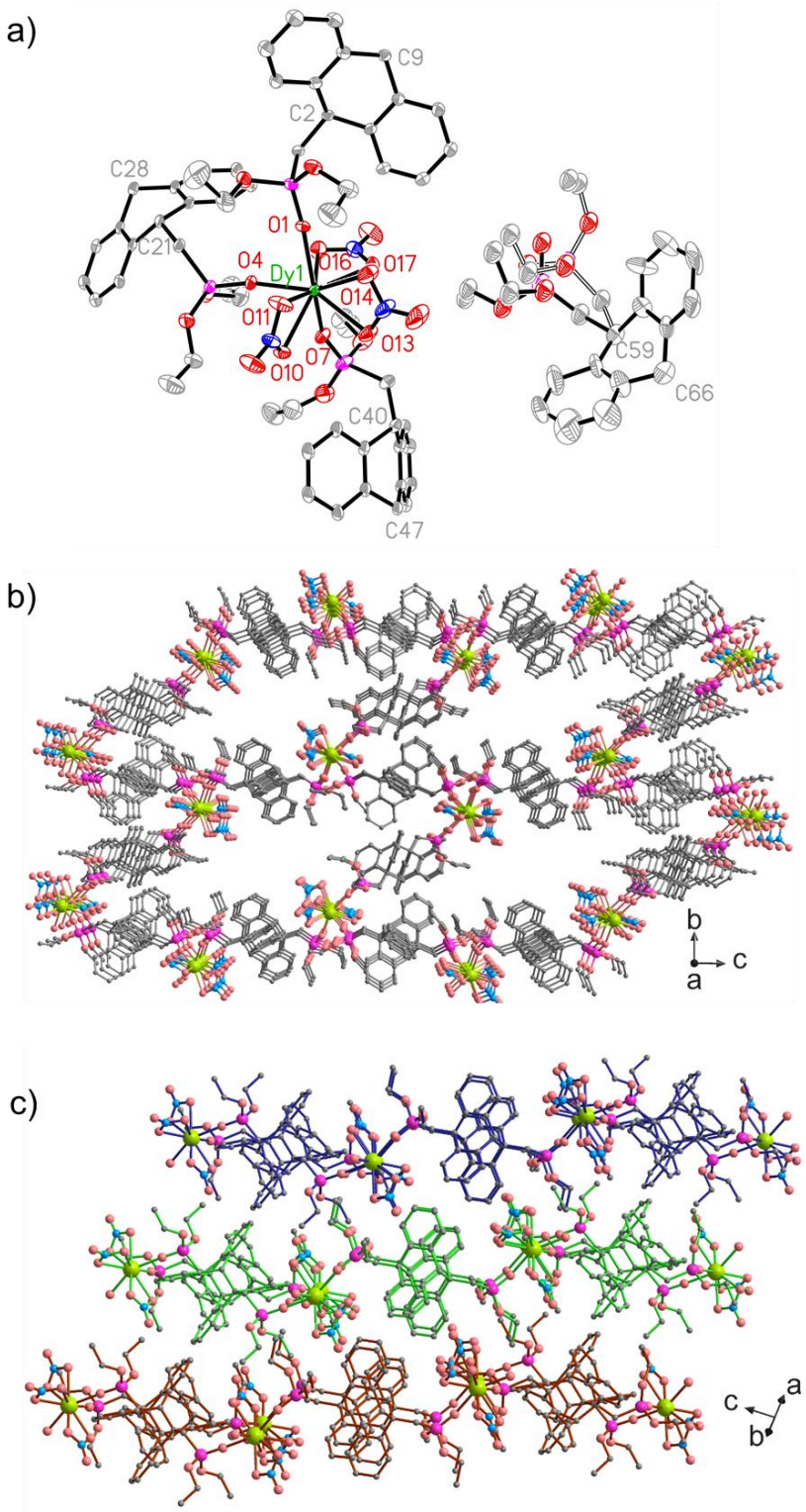

Fig. S5 The structure of **2**. (a) The asymmetric unit with 30% thermal ellipsoids. (b, c) The layer stacking in structure **2** viewed in different directions, the guest depma$_2$-D molecules are omitted to show clearly the channel along the *a*-axis.

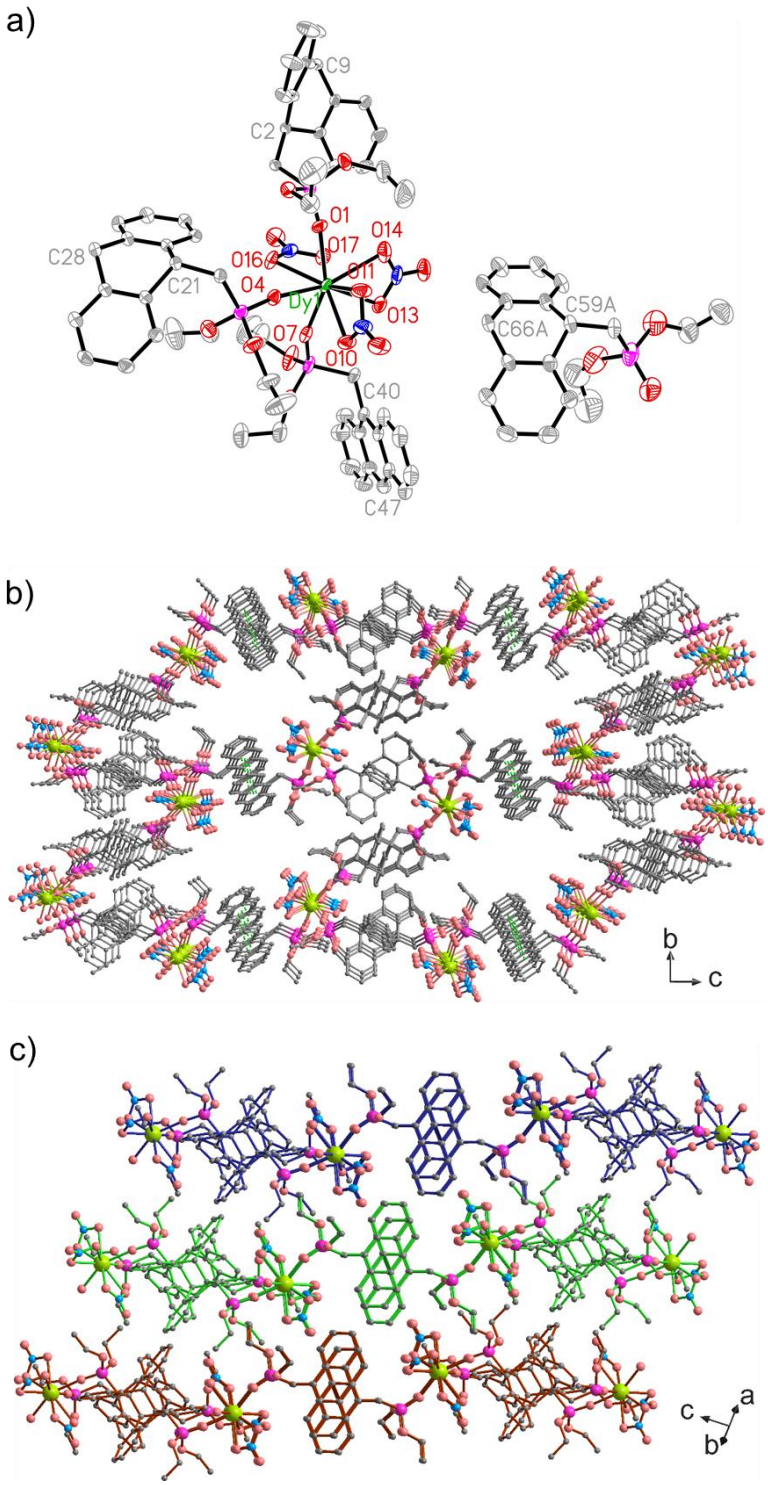

Fig. S6 The structure of **3**. (a) The asymmetric unit with 30% thermal ellipsoids. (b, c) The layer stacking in structure **3** viewed in different directions, the guest depma$_2$-D molecules are omitted to show clearly the channel along the *a*-axis.

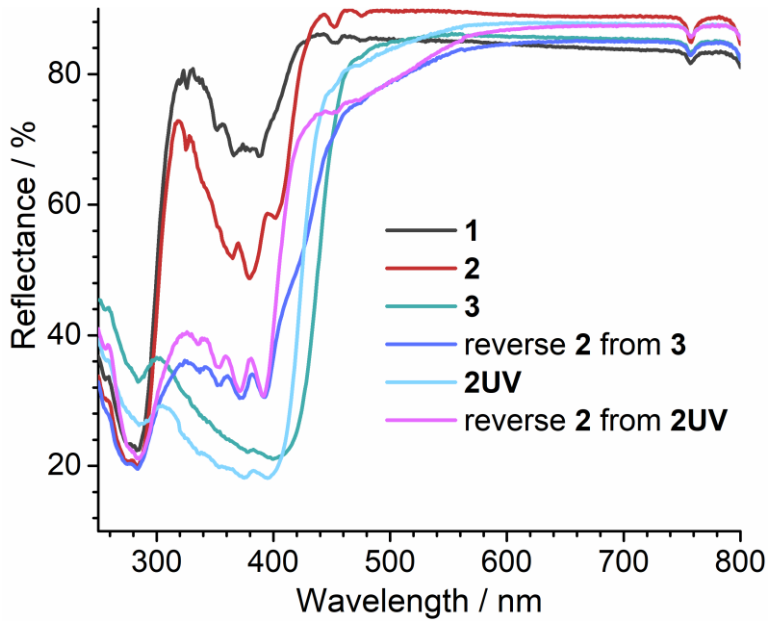

Fig. S7 The UV-Vis diffused reflectance spectra for samples **1**, **2**, **3**, reversed **2** from the exposure of **3** to 365 nm UV light, **2UV** and the reversed **2** by exposing **2UV** to 365 nm UV light.

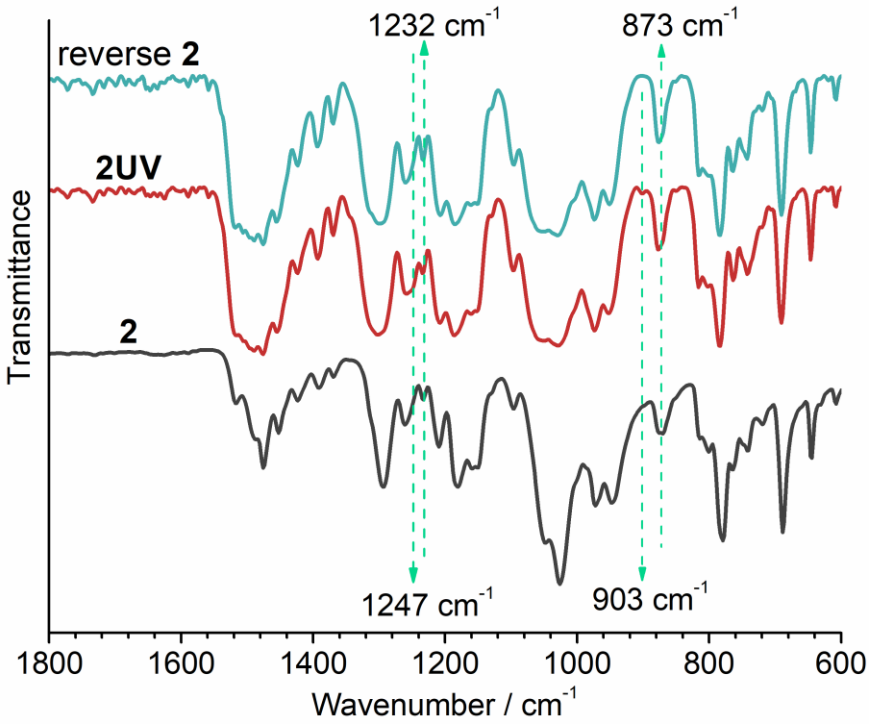

Fig. S8 The FTIR spectra for the samples of **2**, **2UV** given by exposing **2** to 280 nm UV light, and reversed sample **2** by exposing **2UV** to 365 nm UV light.

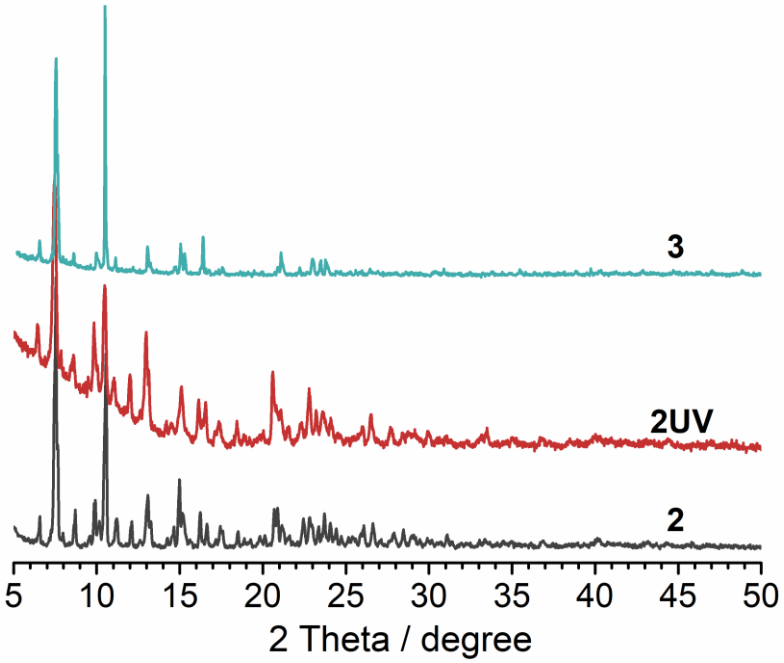

Fig. S9 The PXRD pattern for the sample of **2UV** given by exposing sample **2** to 280 nm UV light, identical to that of **2** and far from that of **3**.

III. Calculation

Table S6 The cell parameters, selective distances and relative energies of optimized structures.

structures	**2**	**2-opt**	**A**	**B**	**C**	**D**	**3**
Space group	$P\bar{1}$	$P\bar{1}$	$P\bar{1}$	$P\bar{1}$	$P\bar{1}$	$P\bar{1}$	$P\bar{1}$
a (Å)	12.017	12.025	11.967	12.146	12.048	12.027	12.132
b (Å)	13.485	13.501	13.234	13.456	13.137	13.505	13.334
c (Å)	23.445	23.455	23.544	23.443	23.266	23.435	23.308
α (°)	90.47	90.60	90.89	90.67	90.45	90.25	90.47
β (°)	97.26	97.18	97.39	96.95	95.91	96.79	96.00
γ (°)	93.18	92.85	94.23	95.13	92.90	94.05	92.72
V (Å^3)	3762.5	3772.9	3686.6	3787.0	3658.0	3770.2	3745.4
Δ*V* (%)	0.0	+0.3	-2.0	+0.6	-2.8	+0.2	-0.5
Dy-O(-P) (Å)	2.288-2.327	2.276-2.321	2.228-2.295	2.257-2.313	2.249-2.284	2.245-2.286	2.290-2.304
Dy-O(-N) (Å)	2.423-2.481	2.406-2.485	2.406-2.552	2.425-2.496	2.436-2.504	2.405-2.513	2.418-2.487
C2-C9A (Å)	1.634	1.634	3.388	1.636	1.636	1.642	1.632
C21-C28B (Å)	1.627	1.631	1.637	3.217	1.633	1.638	1.631
C40-C47C (Å)	1.622	1.637	1.652	1.649	3.552	1.668	3.599
C59-C66D (Å)	1.657	1.628	1.635	1.640	1.636	3.399	1.633
Intralayer Dy-Dy (Å) [(A), (B), (C)]	14.714, 15.212, 14.115	14.737, 15.255, 14.084	14.458, 15.307, 14.115	14.629, 15.173, 14.127	14.512, 15.201, 13.785	14.586, 15.151, 14.206	14.631, 15.248, 13.831
Δ*E* (kJ mol^{-1})		0.0	-8.4	+34.8	-37.3	-1.9	-

Table S7 The parameters, distances and relative energies of optimized structures during dissociation of the $depma_2$-C.

d(C40-C47) (Å)	**1.637**	**2.110**	**2.266**	**2.429**	**2.603**	**3.552**
a (Å)	12.025	12.005	11.976	11.938	11.961	12.048
b (Å)	13.501	13.412	13.321	13.247	13.413	13.137
c (Å)	23.455	23.398	23.363	23.330	23.430	23.266
α (°)	90.60	90.65	91.01	91.40	90.95	90.45
β (°)	97.18	97.27	97.41	97.59	97.47	95.91
γ (°)	92.85	92.98	92.51	91.92	92.58	92.90
V (Å^3)	3772.9	3731.2	3691.39	3653.60	3722.39	3658.0
Δ*V* (%)	0.0	-1.1	-2.2	-3.2	-1.3	-3.0
Intralayer Dy-Dy (Å) [(A), (B), (C)]	14.737, 15.255, 14.084	14.658, 15.233, 14.060	14.642, 15.300, 13.950	14.629, 15.376, 13.841	14.625, 15.293, 14.061	14.512, 15.201, 13.785
Δ*E* (kJ mol^{-1})	0.0	41.6	50.6	48.2	23.0	-37.3

Table S8 The parameters, distances and relative energies of optimized structures during dissociation of the $depma_2$-A.

d(C2-C9) (Å)	**1.634**	**2.104**	**2.155**	**2.317**	**2.593**	**3.388**
a (Å)	12.025	12.124	11.951	11.969	11.983	11.878
b (Å)	13.501	13.636	13.038	13.322	13.332	13.240
c (Å)	23.455	23.475	23.287	23.327	23.467	23.433
α (°)	90.60	90.46	90.38	90.03	90.26	90.88
β (°)	97.18	97.12	97.82	97.34	96.57	97.49
γ (°)	92.85	92.60	92.34	92.51	92.63	92.76
V (Å^3)	3772.9	3667.1	3591.5	3685.6	3720.6	3648.6
Δ*V* (%)	0.0	-2.8	-4.8	-2.3	-1.4	-3.3
Intralayer Dy-Dy (Å) [(A), (B), (C)]	14.737, 15.255, 14.084	14.809, 15.266, 14.154	14.633, 15.312, 13.857	14.825, 15.264, 13.919	14.921, 15.271, 13.898	14.718, 15.359, 13.894
Δ*E* (kJ mol^{-1})	0.0	44.0	66.4	67.6	36.6	-12.2

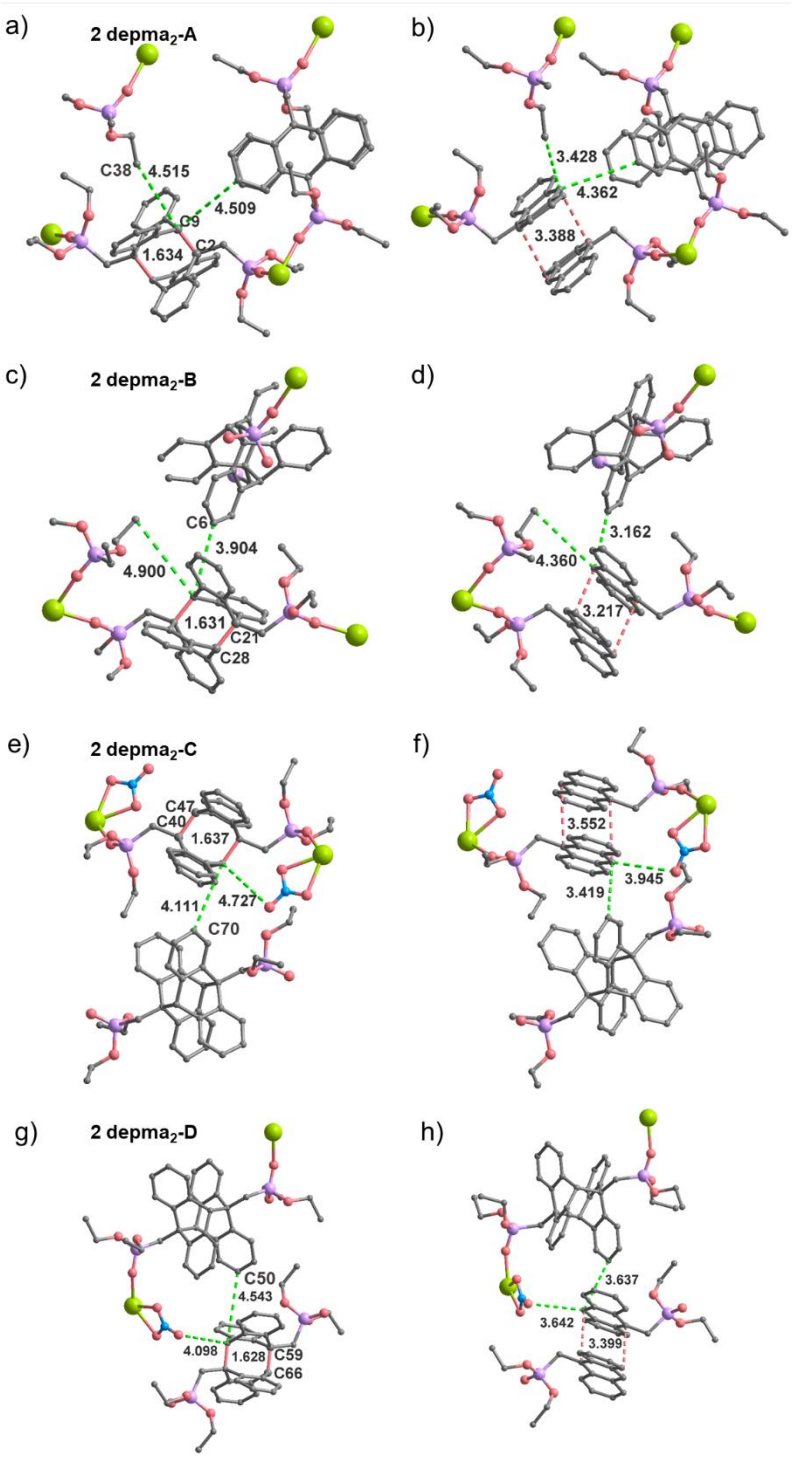

Fig. S10 The optimized structure for **2** (a, c, e, g) and the dissociation of depma$_2$-A (b), -B (d), -C (f) and -D (h) to compare the changes of their local environments. The dianthracene plane of depma$_2$-C faces the intralayer guest of depma$_2$-D in a flexible pore, allowing a long separation by *d*(C40-C47') = 3.552 Å. However, the extension of dissociated depma$_2$-A, B, and D are limited in confined lattice wherein anthracene planes face with adjacent 2D layers.

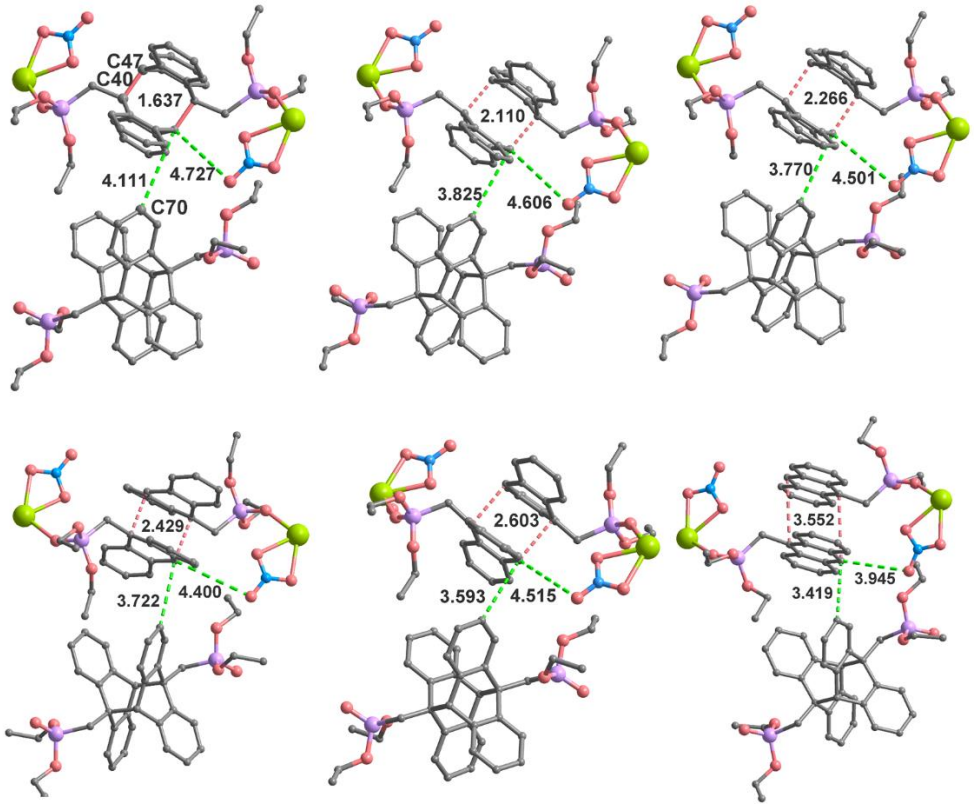

Fig. S11 The simulated dissociation of depma$_2$-C with gradual elongation of C40-C47 distance showing the reduced distance of C47-C70 from 4.111 to 3.419 Å, hinting the increasing steric hindrance from the faced intralayer depma$_2$-D.

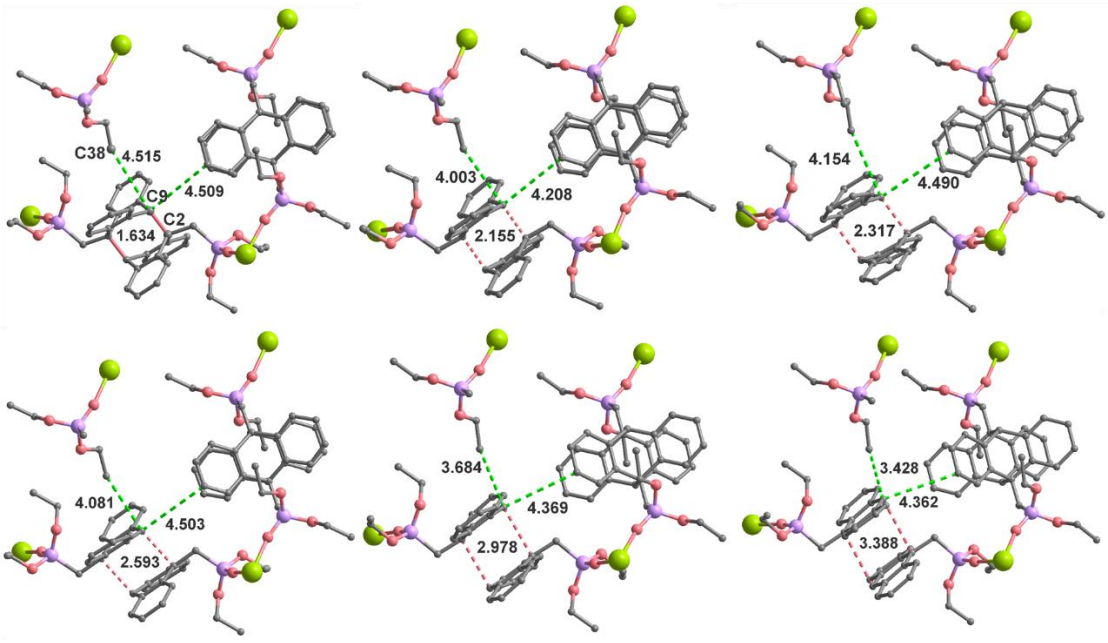

Fig. S12 The simulated dissociation of depma$_2$-A with gradual elongation of C2-C9 distance showing the reduced distance of C9-C38 from 4.515 to 3.428 Å, hinting the increasing steric hindrance from the ethyl of the neighboring 2D layer.

IV. Photoluminescent switching

Table S9 The emission lifetimes at room temperature for compound **1**, **2**, **3** and **2UV** excited at 375 nm for short nanosecond lifetime and at 370 nm for long microsecond lifetime, and absolute photoluminescent quantum yield (PLQY) excited at 365 nm.

compound	λ_{em} / nm	τ_1 / ns	τ_2 / ns	$\tau_{average}$	χ^2	PLQY
1	420	3.83 (63.2 %)	15.2 (36.8 %)	5.29 ns	1.11	12.1(9)
	475	64.6 us	—	64.6 us	1.08	
	574	72.7 us	—	72.7 us	1.16	
2	420	4.10 (66.7%)	15.3 (33.3%)	5.43	1.15	6.7(1)
3	535	42.3	—	42.3	1.12	4.9(1)
2UV	446	0.228(25.87%)	4.30(74.13%)	0.765	1.28	1.6(1)
	526	1.52 (13.12%)	18.5(86.88%)	7.50	1.10	

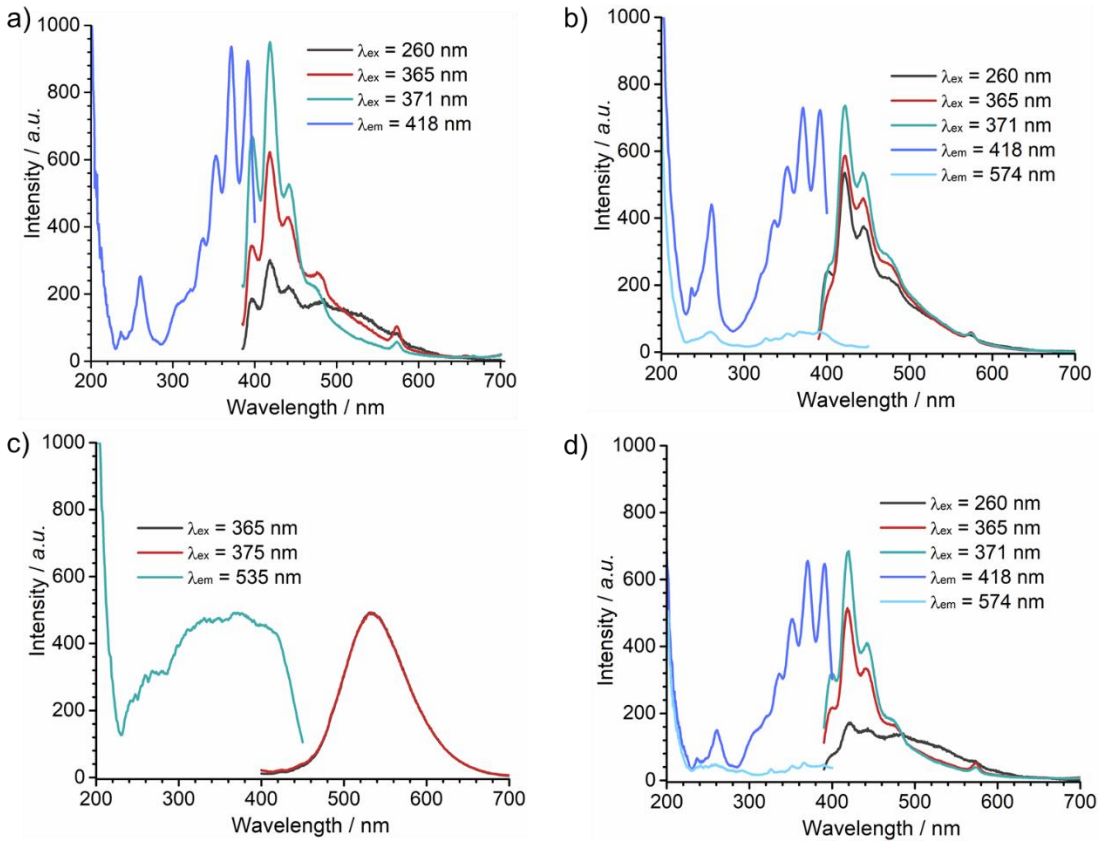

Fig. S13 The excitation and emission spectra for samples **1** (a), **2** (b), **3** (c) and reversed **2** by exposing **3** to 365 nm UV light (d) monitored at depicted wavelength.

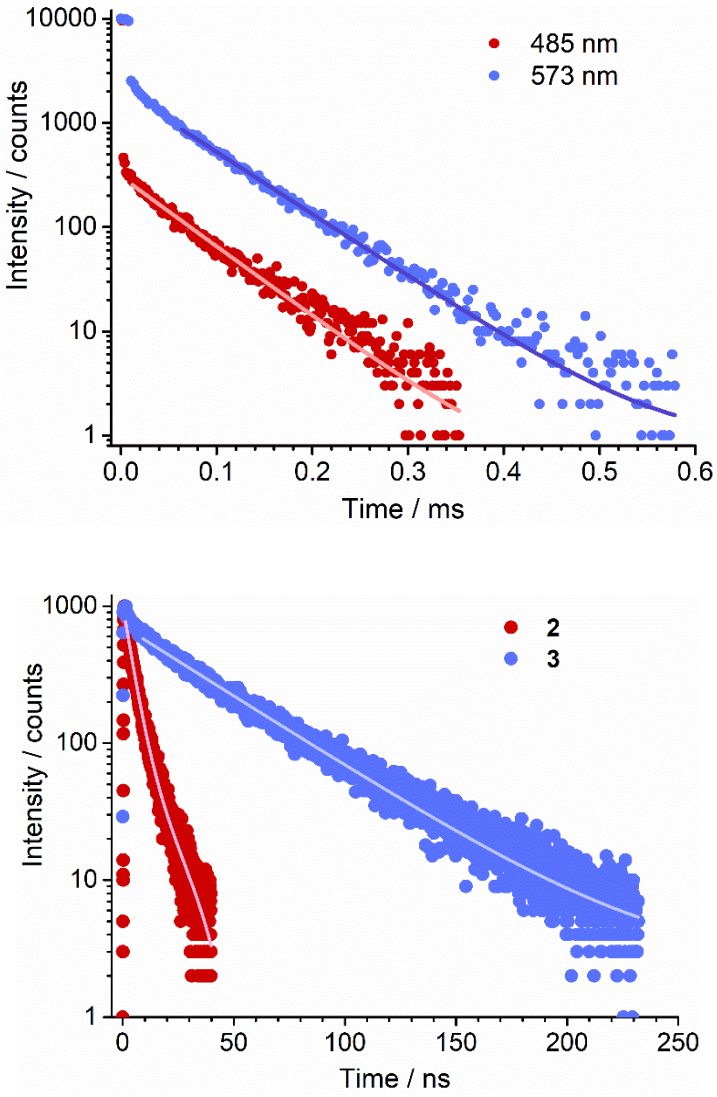

Fig. S14 (Top) The photoluminescent decay curves for **1** monitored at 485 and 573 nm. (Bottom) The photoluminescent decay curves for **2** and **3** monitored at 420 and 535 nm respectively which is fitted to single exponential decay equation.

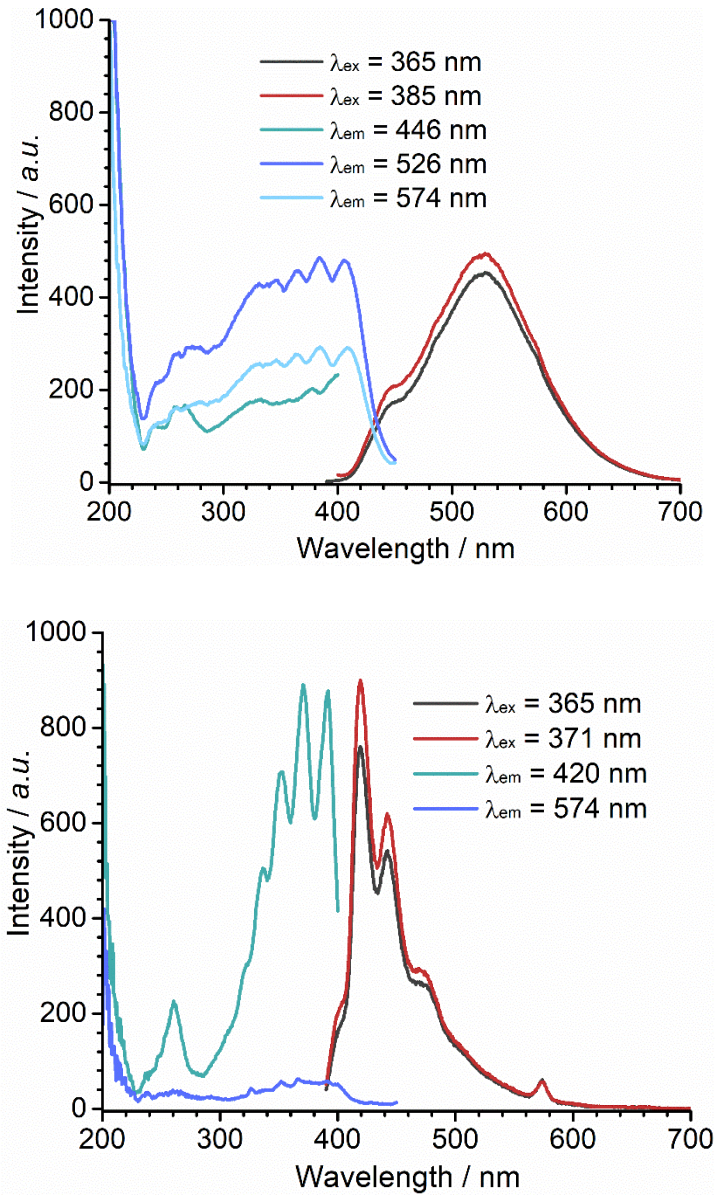

Fig. S15 The excitation and emission spectra for samples **2UV** (top) and reversed **2** by exposing **2UV** to 365 nm UV light (bottom) monitored at depicted wavelength.

V. Photogenerated heterostructured crystal as photonic barcode

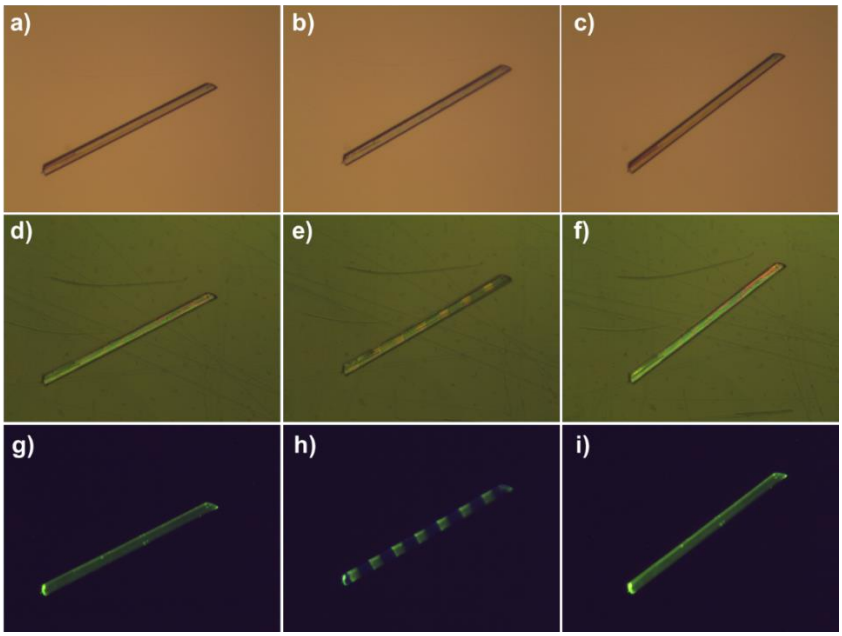

Fig. S16 The photographs for single crystal of pure **3** (a, d, g), heterostructure with sequenced **2** and **3** made by photolithography (b, e, h), reversed **3** by thermal erasure at 140 ºC (c, f, i), taken from the transmission (above) and reflectance (middle) lamp light and UV light (bottom).

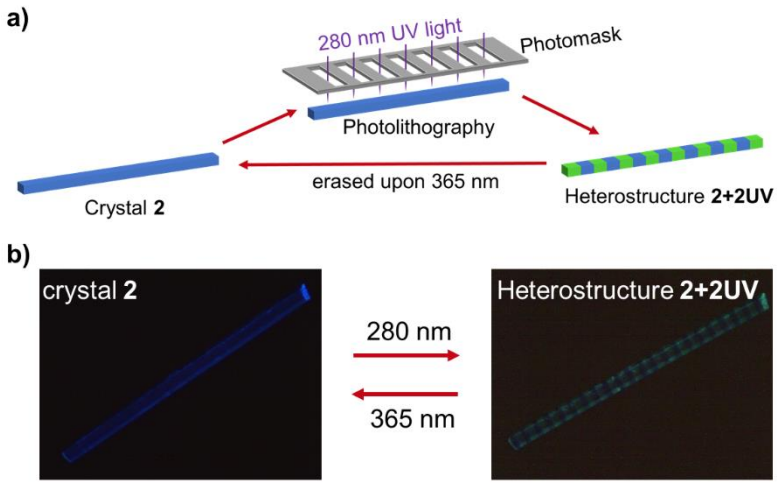

Fig. S17 a) The scheme to show the photolithography process to fabricate and erase the heterostructured crystal **2**+**2UV**. b) The fluorescent graphs showing the switching between the crystal **2** and heterostructured crystal consisting of sequent **2** and **2UV** blocks.

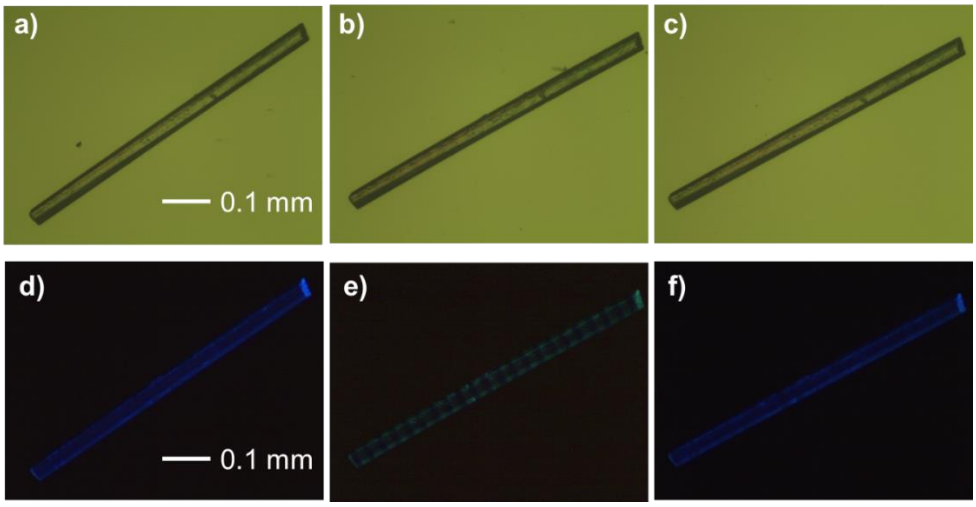

Fig. S18 The photographs for single crystal of pure **2** (a, d), heterostructure with sequenced **2** and **2UV** made by photolithography under 254 nm UV light (b, e), reversed **2** by irradiation with 365 nm UV light for 2 min (c, f), taken from lamp light (top) and UV light (bottom).

VI. Photomechanical effect

Table S10 Some recently reported crystals of coordination compounds showing photomechanical effects.

Compounds (dimension)	Crystal shape	Mechanical effect	reversibility	mechanism	Working temperature	Ref.
$[(Rh)_2(\eta^5\text{-}C_5Me_4n\text{-}C_5H_{11})_2(\mu\text{-}CH_2)_2(\mu\text{-}O_2SSO_2)]$ (0D)	rod	bending	yes	μ-O_2SSO_2 and μ-O_2SOSO photoisomerization	bending at RT, reversed at 105−110°C	5
$[Co(NH_3)_5NO_2]Cl(NO_3)$ (0D)	needle-shaped	bending	yes	nitro–nitrito isomerisation	80−363 K	6-8
	prismatic	exploding, hoping, traveling	no		RT	9
(1,10-phen)Co(3,6-DBSQ)$_2$ (0D)	Thin plate	bending	yes	valence tautomerism	242−265 K	10
$[Ru(NH_3)_4(SO_2)$(3-phenyl-pyridine)$]Cl_2\cdot H_2O$ (0D)	block	peeling	yes	η^1-SO_2 to η^1-OSO photoisomerization	100 K	11
$[Zn_2(benzoate)_4(L^1)_2]$ (0D)	block	poping	no	[2+2] cycloaddition	RT	12
[Zn(bdc)(3F-4spy)] (2D)	rod	bending, twisting	no	[2+2] cycloaddition	RT	13
$Ag(L^1)_2X_2$ (0D)	block	popping, hopping, leaping	no	[2+2] cycloaddition	RT	14
$[Zn(NCS)_2(2F\text{-}4spy)_2]$ (0D)	block	popping	no	[2+2] cycloaddition	RT	15
[Zn(glu)(4-nvp)] (1D)	block	popping	no	[2+2] cycloaddition	RT	16
$[PbI_2$(5-SPym)(DMF)] (1D)	rod	jumping, splitting, rolling, breaking	no	[2+2] cycloaddition	RT	17
U-CB[8]-MPyVB (0D)	rod	bending	no	[2+2] cycloaddition	RT	18
$Zn(acac)_2(6cazpy)_2$ (0D)	plate	bending	yes	cis-trans isomerization	RT	19
$[Cu(CNAB)_4][PF_6]$ (0D)	rod	bending	yes	cis-trans isomerization	RT−333 K (60 °C)	20
$[Dy(depma_2)_{1.5}(NO_3)_3]\cdot 0.5$ depma$_2$ (2D)	rod	bending, contraction	yes	[4+4] cycloaddition	RT−423 K (150 °C)	This work

1,10-phen = 1,10-phenanthroline, 3,6-DBSQ = anion-radical of 3,6-di-tert-butyl-o-benzoquinone, H_2bdc = 1,4-benzenedicaboxylic acid, L^1 = 4-styrylpyridine (4spy), X = NO_3^-; L^1 = 2′-fluoro-4-styrylpyridine (2F-4spy), X = BF_4^-, ClO_4^-; L^1 = 3′-fluoro-4-styrylpyridine (3F-4spy), X = BF_4^-, ClO_4^- and NO_3^-, H_2glu = glutaric acid, 4-nvp = 4-(1-naphthylvinyl)pyridine, 5-Spym = trans-5-Styrylpyrimidine, acac$^-$ = acetylacetonate, 6cazpy = 4-(4-(6-Hydroxyhexyloxy) phenylazo, CNAB = 4-isocyanoazobenzene. RT = room temperature

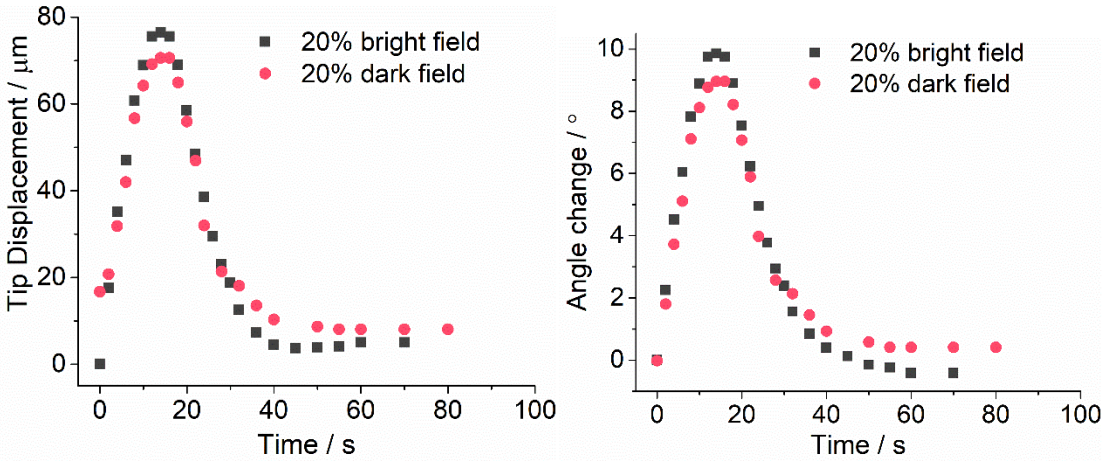

Fig. S19 The tip displacement (left) and deviation angle (right) during the photobending processes upon irradiation with 365 nm UV light (20% power) for selected rod-like crystal **C**.

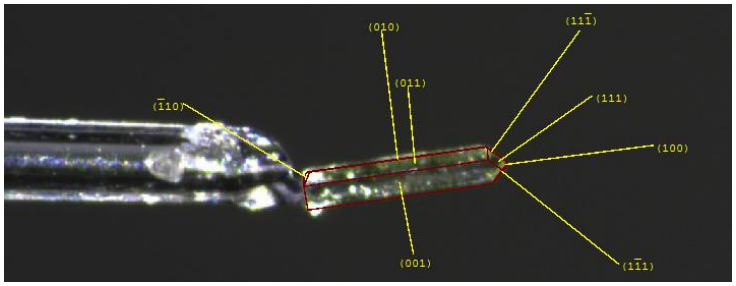

Fig. S20 The crystal face index for one rod-like crystal of **3**.

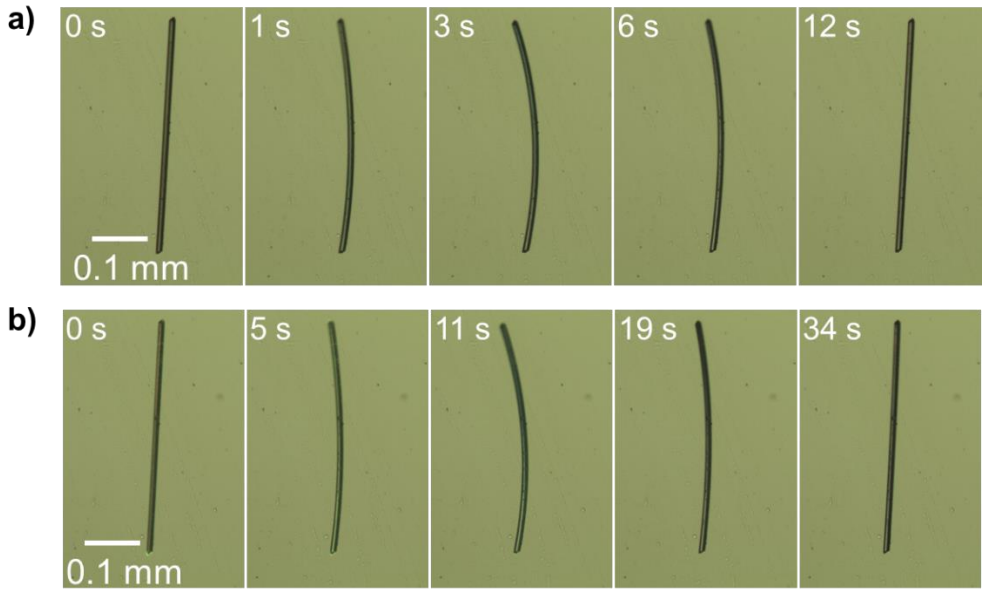

Fig. S21 The photobending for crystal **D** of compound **3** upon irradiation with 365 nm UV light (20% power) at 140°C (a) and room temperature (b).

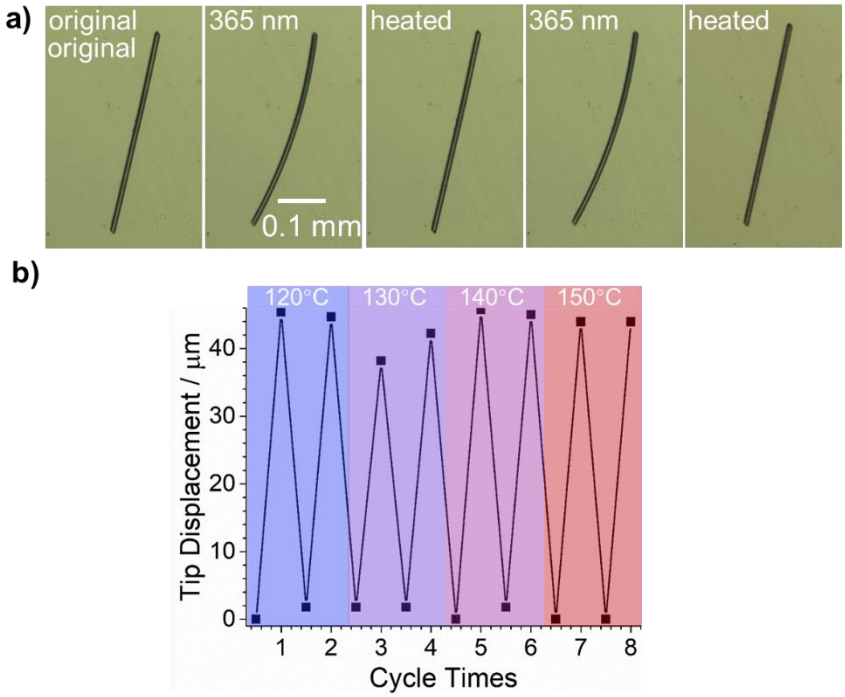

Fig. S22 a) The pictures for the repeated photobending deformation for crystal **D** through alternate irradiation with 365 nm UV light (20 % power) for the first 3s and thermal annealing at 140°C for 3 min. b) The tip displacements for the reversible bending of crystal **D** of **3** up to 8th times driven by alternative irradiation with 365 nm UV light in 20% power for 3 s and thermal annealing at 120°C for 12 min, 130°C for 5 min, 140°C for 3 min, 150°C for 2 min.

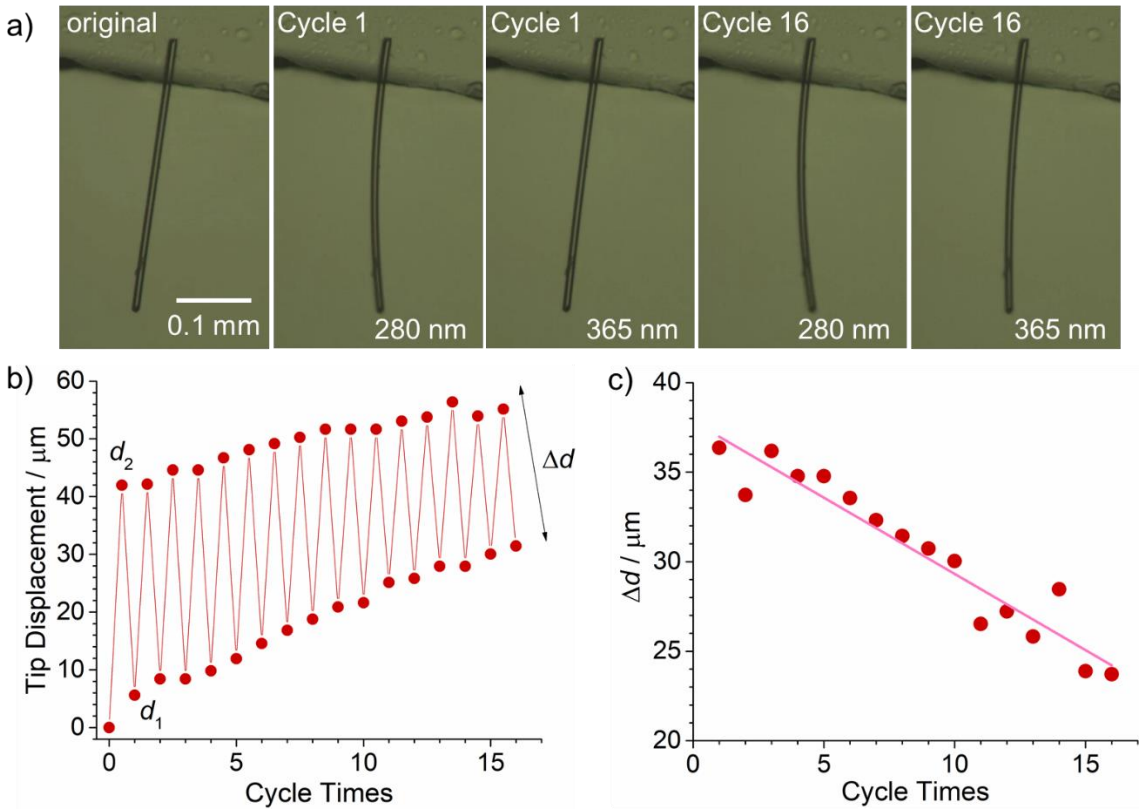

Fig. S23 The pictures (a) and tip displacements (b, c) for the repeated photobending for crystal **F** of compound **2** through irradiation with alternate 280 nm in 20 % power for 8 s and 365 nm UV light in 20% power for 10 s.

VII. References:

1. J.-C. Liu, X.-D. Huang, Q. Zou, S.-S. Bao, X.-Z. Wang, J.-Y. Ma and L.-M. Zheng, *J. Mater. Chem. C,* 2020, **8**, 7369–7377.
2. SAINT. Program for Data Extraction and Reduction. Siemens Analytical X-ray Instruments. Madison, WI, 1994–1996.
3. L. Krause, R. Herbst-Irmer, G.M. Sheldrick and D. S. Ike, *J. Appl. Cryst*., 2015, **48**, 3–10.
4. G. M. Sheldrick, *Acta Cryst*., 2015, **C71**, 3–8.
5. H. Nakai, K. Matsuba, M. Akimoto, T. Nozaki, T. Matsumoto, K. Isobe, M. Iriee and S. Ogo, *Chem. Commun*., 2016, **52**, 4349–4352.
6. A. A. Sidelnikov, S. A. Chizhik, B. A. Zakharov, A. P. Chupakhin and E. V. Boldyreva, *CrystEngComm,* 2016, **18**, 7276–7283.
7. S. Chizhik, A. Sidelnikov, B. Zakharov, P. Naumov and E. Boldyreva, *Chem. Sci*., 2018, **9**, 2319–2335.
8. S. Chizhika, A. Sidelnikov, B. Zakharov and E. Boldyreva, *Materials Today: Proceedings,* 2019, **12**, 35–38. 2019
9. P. Naumov, S. C. Sahoo, B. A. Zakharov and E. V. Boldyreva, *Angew. Chem. Int. Ed*., 2013, **52**, 9990–9995.
10. M. P. Bubnov, K. A. Kozhanov, N. A. Skorodumova and V. K. Cherkasov, *Inorg. Chem*., 2020, **59**, 6679–6683.
11. J. M. Cole, J. d. J. Velazquez-Garcia, D. J. Gosztola, S. G. Wang and Y.-S. Chen, *Chem. Mate*r., 2019, **31**, 4927–4935.
12. R. Medishetty, A. Husain, Z. Bai, T. Runčevski, R. E. Dinnebier, P. Naumov, J. J. Vittal, *Angew. Chem. Int. Ed*., 2014, **53**, 5907–5911.
13. Y.-X. Shi, W.-H. Zhang, B. F. Abrahams, P. Braunstein and J.-P. Lang, *Angew. Chem. Int. Ed*., 2019, **58**, 9453–9458.
14. R. Medishetty, S. C. Sahoo, C. E. Mulijanto, P. Naumov and J. J. Vittal, *Chem. Mater*., 2015, **27**, 1821–1829.
15. C. E. Mulijanto, H. S. Quah, G. K. Tan, B. Donnadieu and J. J. Vittal, *IUCrJ,* 2017, **4**, 65–71.
16. B. Dutta, C. Sinha and M. H. Mir, *Chem. Commun*., 2019, **55**, 11049–11051.
17. B. B. Rath and J. J. Vittal, *J. Am. Chem. Soc*., 2020, **142**, 20117–20123.
18. J.-s. Geng, L. Mei, Y.-y. Liang, L.-y. Yuan, J.-p. Yu, K.-q. Hu, L.-h. Yuan, W. Feng, Z.-f. Cha and W.-q. Shi, *Nat. Commun*., 2022, **13**, 2030.
19. Y. Guo, Y. Hao, L. Gao and H. Hao, *Crystals,* 2020, **10**, 92.
20. A. K. Bartholomew, I. B. Stone, M. L. Steigerwald, T. H. Lambert and X. Roy, *J. Am. Chem. Soc.,* 2022, **144**, 16773−16777.